



Bidirectional wakes over complex terrain using SCADA data and wake models

Nanako Sasanuma¹, Akihiro Honda², Christian Bak³, Niels Troldborg³, Mac Gaunaa³ and Morten Nielsen³, Teruhisa Shimada¹

- 5 ¹Graduate School of Science and Technology, Hirosaki University, Bunkyo-cho 3, Hirosaki, 036-8561, Japan
²Aomori Public University, Department of Management and Economics, Aomori, Aomori, Japan, 030-0196, Japan
³DTU Wind and Energy Systems, Technical University of Denmark, Roskilde, 4000, Denmark

Correspondence to: Nanako Sasanuma (h22ds203@hirosaki-u.ac.jp)

Abstract.

- 10 We investigate bidirectional wake effects between the same type of two wind turbines in a hill region in northern Japan using Supervisory Control and Data Acquisition (SCADA) data and validate the performance of 12 wake models. The two turbines are located 3.7 times a rotor diameter apart with a different elevation of half of a rotor diameter. We identify the wake effects in terms of wind speed ratio, which is defined as a ratio of wind speed at the downstream wind turbine to that at the upstream wind turbine. By comparing the conditions according to the operating state of the upstream wind turbine, the wakes are clearly detected as
- 15 minimum wind speed ratios for northeasterly and southwesterly winds. The wind speed ratio decreases with inflow wind speed below the rated wind speed. Increase in turbulence intensity and decrease in power output are greater for southwesterly wind than for northeasterly wind because of the combined effects of the turbine-induced wake and the terrain-induced reduction in wind speed. Then, we compare the simulated wakes from the validate the wake models implemented in PyWake software by using simulated wind fields derived from Wind Atlas Analysis and Application Program (WAsP) Computational Fluid Dynamics (CFD). The wind
- 20 speed ratios derived from the models show strong dependence on inflow wind speed, reflecting the thrust curve used in the engineering wake models. The wake models commonly overestimate the reduction in wind speed for northeasterly wind and underestimate it for southwesterly wind. Thus, this study demonstrates that additional effects of topography alter the wake effects.

1 Introduction

- Wake generated by neighbouring wind turbines is critical issue for the design of wind power plant layout. We need to manage the
- 25 wake effects. Otherwise, wakes can negatively impact downstream turbines by reducing wind speeds and subsequent power output and by increasing turbulence intensity and resulting higher fatigue loads. Moreover, over complex terrain, the topography additionally alters airflow influenced by wakes. An increasing number of wind turbines are being installed in complex terrains, such as hills, escarpments, valleys, and gorges, with decreasing in flat terrain suitable for wind farms. Although installation in complex terrain poses logistic challenges, strong winds induced by topographic effects offer an advantage for wind resource (e.g., Yamaguchi
- 30 et al., 2024). Thus, the combined effects of wake and terrain further complicate the optimization of the performance and control strategies of wind farm.

- Wind measurements are essential for understanding of wake phenomena (e.g., Rhodes and Lundquist, 2013; Hansen et al., 2016; El-Asha et al., 2017; Mittelmeier and Kühn, 2017; Astolfi et al., 2018; Han et al., 2018). Among observational data, supervisory control and data acquisition (SCADA) provides an advantage on concurrent analysis of the actual conditions of wind at the hub
- 35 height and of operating states of wind turbines. In addition to SCADA data, external measurements, such as light detection and ranging (LiDAR) measurements, are widely used to observe wakes. Rhodes and Lundquist (2013) indicated dependence of wake effects on inflow wind speed. Combined use of various observations enables to further investigate the vertical structure of reduction in wind speed and increase in turbulence intensity (Rhodes and Lundquist, 2013), the impact of wakes on power generation in flat



terrain (El-Asha et al., 2017) and in complex terrain (Han et al., 2018), and turbulence intensity depending on wake effects
40 (Mittelmeier and Kühn, 2017). Astolfi et al. (2018) used SCADA data with numerical simulation to demonstrate that the wake
structures are distorted by the surrounding terrain and that wind speed recovery is quicker over complex terrain than over flat terrain.
Using SCADA data in conjunction with external equipment is an effective method for wake detection. However, external equipment
involves high costs and offers for operation and maintenance and operation periods are often limited.

Simulations enable to effectively analyse the wake and complement observations (Göçmen et al., 2016; Carbajo Fuertes et al.,
45 2018; Bastankhah and Porté-Agel, 2014; Troldborg et al., 2022). Göçmen et al. (2016) suggest that wake models have different
advantages in terms of usability, accuracy, quantity and quality of inputs, and computational costs by evaluating utilization of the
six wake models with SCADA data in Sexbierum (onshore) and Lillgrund (offshore) wind farms. Gaussian wake model was
validated by two pulsed scanning Doppler lidars mounted on the nacelle by measuring both the incoming flow and the downstream
wake (Carbajo Fuertes et al., 2018). Bastankhah and Porté-Agel (2014) validated a Gaussian model for the reproducibility of wind
50 speed at the downstream wind turbine by wind-tunnel measurements and the large-eddy simulations (LES) data. Troldborg et al.
(2022) found that the turbines performance of wind turbines in complex terrain is highly variable compared to that in flat
homogeneous terrain by using LES simulation. Wake models have been validated by various methods; however, a limited number
of studies have validated simulated wakes over the complex terrain.

To investigate basic behaviour of wakes over complex terrain, we have focused on a site in northern Japan (Fig. 1a; Sasanuma and
55 Honda, 2022; Sasanuma and Honda, 2024). Because the region near Cape Tappi is characterized by abundant wind resources and
steep topography, this site has been a research site for operation of wind turbines since the first utility-scale wind farm in Japan was
built in 1991 (Fig. 1b; e.g., Ushiyama, 1999; Inomata et al., 1999; Enomoto et al., 2001; Fujikawa et al., 2002; Hasegawa et al.,
2003). Annual mean wind speed at the site is above 8 m s^{-1} , with prevailing winds in east-west direction over the mountainous
terrain (Sasanuma and Honda, 2022). Strong westerly winds dominate in winter due to the Siberian high, whereas easterly winds
60 intermittently blow in summer due to the Okhotsk high (Shimada et al., 2014). The southwesterly winds result in a pronounced
wake effect with a 24% reduction in wind speed and a 22% increase of turbulence intensity at the downstream wind turbine
(Sasanuma and Honda, 2022). Sasanuma and Honda (2024) indicated that engineering wake models generally underestimate the
reduction in wind speed in the wakes compared with those observations.

However, we need to further explore the wakes between two wind turbines for evaluating wake effects induced by multiple
65 upstream of wind turbines or by wind power plants. First, we need to compare bidirectional wake effects between the two wind
turbines to clarify the differences in wake effects over the complex terrain according to the wind direction. Sasanuma and Honda
(2022; 2024) investigated wake effects only one-way direction between the two turbines. Wake effects in the other direction remain
unclear. Moreover, we need to look into the dependence of wake effects on inflow wind speed over complex terrain. Second, we
need to validate the performance of each wake model by comparing the simulated results with the observed results by SCADA data
70 and to clarify the dependence of simulated wake effects on inflowing wind speed. The validation of engineering wake models is
still insufficient. By comparing the mutual wake effects derived from wake models, we need to identify similarities and differences
between the wake models.

We investigate the bidirectional wakes behavior between two wind turbines over the complex terrain using the SCADA data and
validate the performance of engineering wake models with the SCADA data. We specifically address the following two issues: (1)
75 to identify the wake effects at the downstream wind turbine by comparing the conditions with and without the operation of the
upstream wind turbine and evaluate the wake effects in terms of reduction in wind speed, turbulence intensity, and power output.
(2) to validate simulated wakes by engineering wake models against the SCADA data. This research highlights the effectiveness of
using SCADA data to investigate flow characteristics arising from both topography and wakes of a wind turbine. Moreover, we
demonstrate the potential to utilize SCADA data and provide much information.

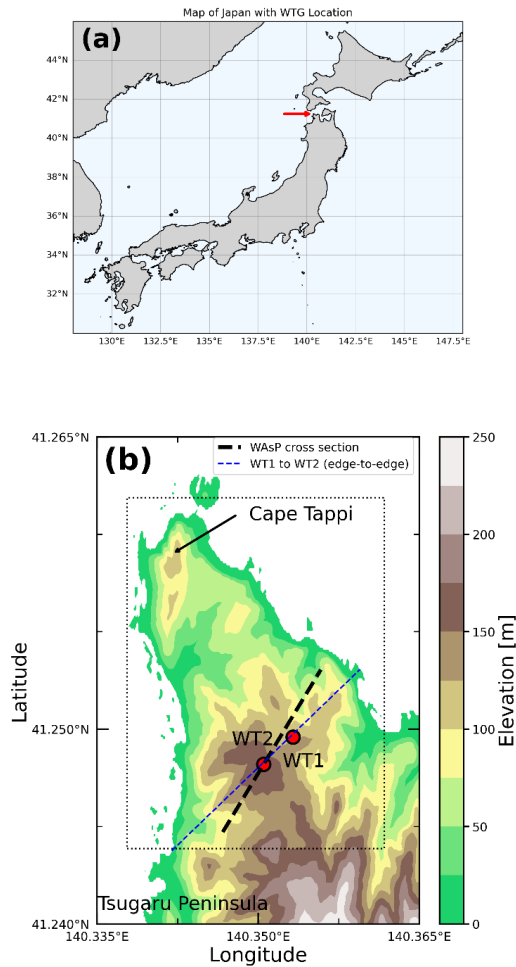


80 Section 2 describes the wind turbines, the SCADA data, the wind condition at the site, the methodology to detect of wake effects, and the wake simulation. Section 3 analyses the SCADA data to examine the wake effects and compares the observed results with the simulated results by engineering wake models. Section 4 presents the summary and conclusions.

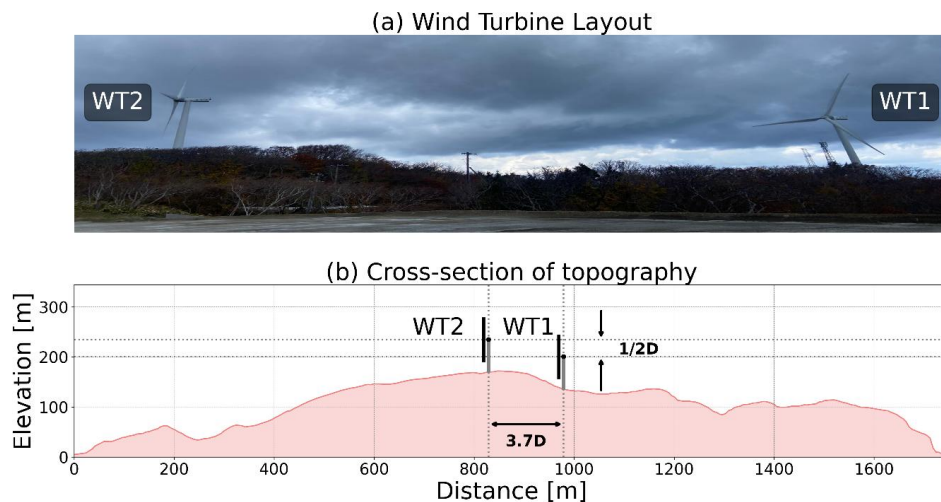
2 Data and Methodology

2.1 Two wind turbines

85 This study focuses on mutual wake effects between two wind turbines (WT1 and WT2) located near the northern tip of the Tsugaru Peninsula, Japan (Fig. 1a and 1b). Their original model is J82-2.0 manufactured by Japan Steel Works with a hub height of 65 m and a rotor diameter of 83.3 m (Fig. 2a). Rated power output is 1.675 MW. Full operation started in 2010. The two wind turbines are located almost in a southwest-northeast direction (Fig. 1b) and the horizontal distance between the two turbines is 3.7 times the rotor diameter (Fig. 2b). WT1 and WT2 are located at an altitude of 132 m and 169 m, respectively. The difference in elevation
90 correspond to half a rotor diameter. In a cross-section along the line connecting the two turbines, WT2 is located at the highest location (Fig. 2b). The surrounding terrain is covered by bush trees (Fig. 2a).



95 **Figure 1.** (a) Location of the study site in Japan. (b) The topography of the study site (color shading) and the locations of wind turbines 1 (WT1) and wind turbine 2 (WT2) (red circles). The blue dashed line represents the line connecting the two wind turbines to show the topography in Fig. 2b. The black dashed line denotes the location of the vertical cross sections analysed in Fig. 14. The square enclosed by the dotted line is a 2km × 2km computational domain for WAsP CFD.



100

Figure. 2 (a) Photo of the two wind turbines. (b) Cross section of the topography along the line connecting the two wind turbines shown in Fig. 1b. The elevation data are obtained from the website of Geospatial Information Authority of Japan (Geospatial Information Authority of Japan, 2025).

2.2 SCADA

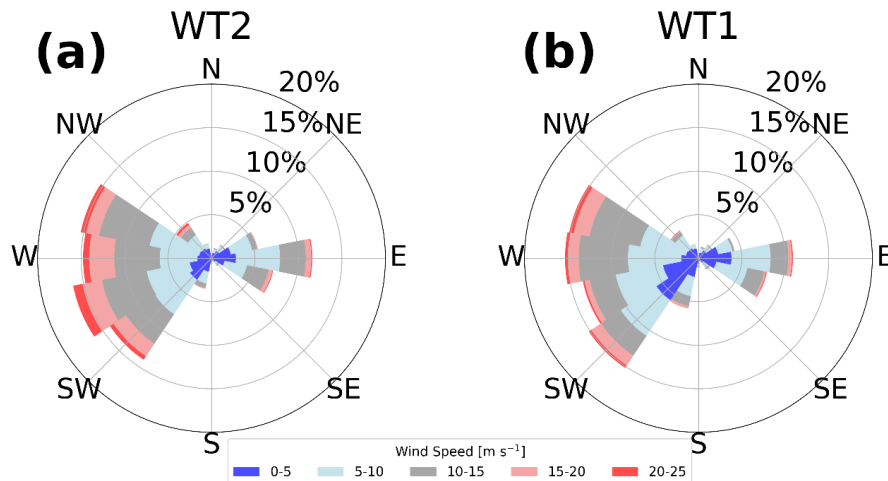
105 We used 10-minute mean SCADA data of the two wind turbines from 5 September 2015, to 31 December 2017. The original data are sampled at an interval of 1 second. The dataset includes wind speed, wind direction, standard deviation of wind speed, nacelle direction, blade pitch angle, rotor speed, and power output. The wind data are measured by a wind vane and a three-cup type anemometer mounted at the rear of the nacelle. Turbulence intensity is defined as standard deviation of wind speed divided by mean wind speed. We applied the following data selection and correction to the SCADA data. First, we used the data with the yaw misalignment, a difference between wind direction and nacelle direction, within plus or minus 10° . A total of 80% of the data satisfy this condition. Second, we corrected the discrepancy between the wind conditions behind the rotating blades and the ones at the upstream side of the wind turbine due to turbulence caused by the blade rotation. In this paper, we applied a method to correct wind direction and wind speed measured on the nacelle without any external data (Appendix A)

110

2.3 Wind farm climate

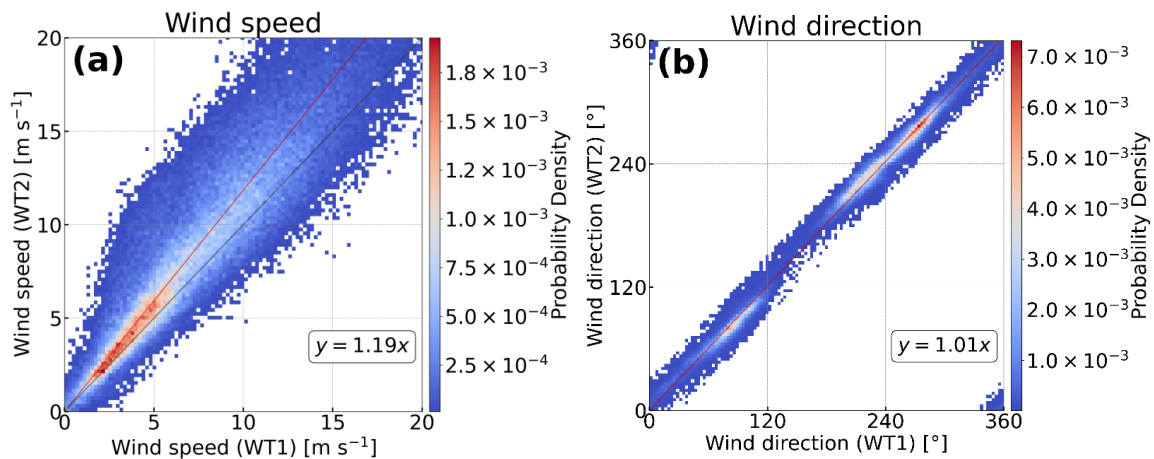
115 We present the wind climate at the two wind turbines from the SCADA data (Figs. 3 and 4). The westerly wind and easterly wind commonly dominate at WT1 and WT2 (Fig. 3). Westerly winds are stronger than easterly wind and the wind direction from southwest to west-northwest account for 60% at WT2 (Fig. 3a) and 59% at WT1 (Fig. 3b). WT2 exhibits higher speeds than WT1 because WT2 is located on top of a hill and wind is accelerated on the hill (Yamaguchi et al., 2002). The frequency exceeding 15 m s^{-1} amount to 8% at WT1 and 14% at WT2 in all wind direction. The wind speeds at WT1 and WT2 show significant correlation (Fig. 4a). Wind speeds at WT2 show 20% higher than those at WT1. Wind directions at WT1 and WT2 are in good agreement (Fig. 4b). The data are concentrated in the easterly wind (90° – 100°) and the westerly wind (220° – 260°), which is consistent with Fig. 3. This means that the dominant wind blows almost along the line connecting the two turbines and that the locations of the two wind turbines are suitable for analysing mutual wake effects between the wind turbines.

120



125

Figure 3. Wind roses derived from the SCADA data of (a) WT2 and (b) WT1. The frequencies are shown at every 5 m s^{-1} with different colors. Wind direction is defined as the direction from which the wind blows.



130 **Figure 4.** Scatter plots of (a) wind speed and (b) wind direction between WT1 and WT2 from the SCADA data. The color represents the data density. The red lines in (a) and (b) are the linear regression lines, shown by the equation in the figures. The black line in (a) represents a 1:1 line.

2.4 Detection of wake effects

To assess the wake effects generated by the upstream wind turbines only based on SCADA data, we divided the data into two categories on the basis of the operating state of the upstream wind turbine: “no-wake conditions” and “wake conditions” (Sasanuma and Honda, 2022; Sasanuma and Honda, 2024). “No-wake conditions” mean that the upstream wind turbine is not operating and “wake conditions” mean that the upstream wind turbine is in operation. Sasanuma and Honda (2024) identified the operating states of wind turbines by a combination of rotor speed, blade pitch angle, and power output. We found that we can distinguish whether the turbine is operating or not only by the blade pitch angle. By imposing the condition that the blade pitch angle is within $\pm 3^\circ$, we can extract the data when the wind turbine is in operation below the rated wind speed. The blade pitch angle is 90° when the turbines

140



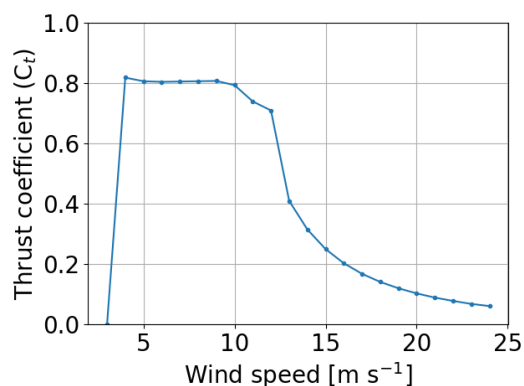
is in non-operation. When considering wake conditions, we focus on the data with wind speeds ranging from the cut-in wind speed and the rated wind speed. In this range, wake effects are maximized, and, above the rated wind speed, wake effects are reduced by the blade pitch control (e.g., El-Asha et al., 2017; Dilip and Porté-Agel, 2017; Duncan et al., 2020). Thus, by comparing no-wake conditions and wake conditions, we can statistically analyse the influence of wakes generated by the upstream wind turbine on mean
145 wind speed, turbulence intensity, and power output at the downstream wind turbine.

2.5 Wind speed ratios

To analyse mutual wake effects between the two wind turbines, we define a wind speed ratio of wind speed at the upstream wind turbine to that at the downstream wind turbine. We should notice that the definition of the wind speed ratio differs by wind direction. When northeasterly wind dominates, wakes induced by WT1 influence WT2. Thus, the wind speed ratio is defined as the ratio of
150 wind speed at WT2 (WS_2) to that at WT1 (WS_1). When southwesterly wind dominates, wakes induced by WT2 influence WT1. Thus, the wind speed ratio is defined as the ratio of wind speed at WT1 (WS_1) to that at WT2 (WS_2). For the respective northeasterly wind and southwesterly wind, we compare the wind speed ratio in wake conditions and in no-wake conditions to evaluate the wake effects.

2.6 Flow wake models

We utilized the Wind Atlas Analysis and Application Program (WAsP; Beckman, 2012) Computational Fluid Dynamics (CFD) and PyWake (Pedersen et al., 2018) for validation of the observed wind and wakes. WAsP CFD is a nonlinear model based on EllipSys 3D code, which is a multiblock finite volume discretization of incompressible Reynolds Averaged Navier-Stokes (RANS) equations. The model operates under the assumption of a neutral atmospheric stability. We used WAsP CFD for evaluating the influence of topography on wind flow. Computational domain is shown in Fig. 1b. The horizontal grid interval is 90m and the
160 elevation map used is spaced at 5m intervals (Geospatial Information Authority of Japan, 2025). The data are output at 13 levels from 5 m to 300 m (5, 10, 20, 33, 48, 65, 80, 100, 120, 150, 200, 250, and 300 m) from the ground level. The upper boundary of the computational domain is 7000 m. PyWake is an open-source wind farm simulation tool written in Python. This tool simulates the flow with wind turbines, at a hub height by incorporating engineering wake models. PyWake has 12 wake models (Appendix B): 11 engineering approaches (e.g. Bastankhah and TurboGaussian) and a linearized Reynolds-averaged Navier-Stokes approach
165 (Fuga). We used the coefficient curve of the V80 2MW wind turbine because the rated power output of this wind turbine is closest to that of the wind turbines in this study among turbine models available in PyWake. The thrust coefficient curve of the V80 is shown in Fig. 5. In this study, we discuss similarities and differences between the wake models for mutual wind directions when a typical thrust curve is used.



170 **Figure 5.** Thrust coefficient as function of wind speed from V80 wind turbine.



3 Results

3.1 Observational results

We examine the wind speed ratios to evaluate wake effects caused by the upstream wind turbine. Figure 6 shows wind speed ratio
175 between the two wind turbines without any categorizations. The wind speed ratios are generally above 1.0 in Fig. 6a and below 1.0
in Fig. 6b, whereas we can identify V-shaped curve or significant reductions in wind speed ratio at around 45° and 225° (light blue
shading in Figs. 6a and 6b). The ranges of these significant reductions are approximately $\pm 10^\circ$ on both sides of the wind directions.
We can see no other significant reduction. The wind directions of 45° and 225° nearly correspond to the direction of the line
connecting the two wind turbines located in the northeast-southwest direction (Fig. 1b). Thus, mutual wakes between the wind
180 turbines cause the significant reductions in wind speed ratio. We focus on the wind directions of 45° and 225° in the following
analyses.

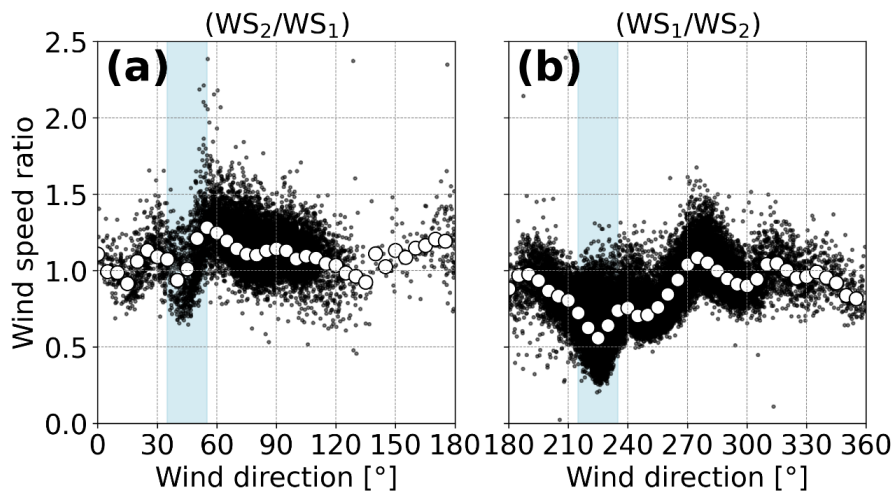


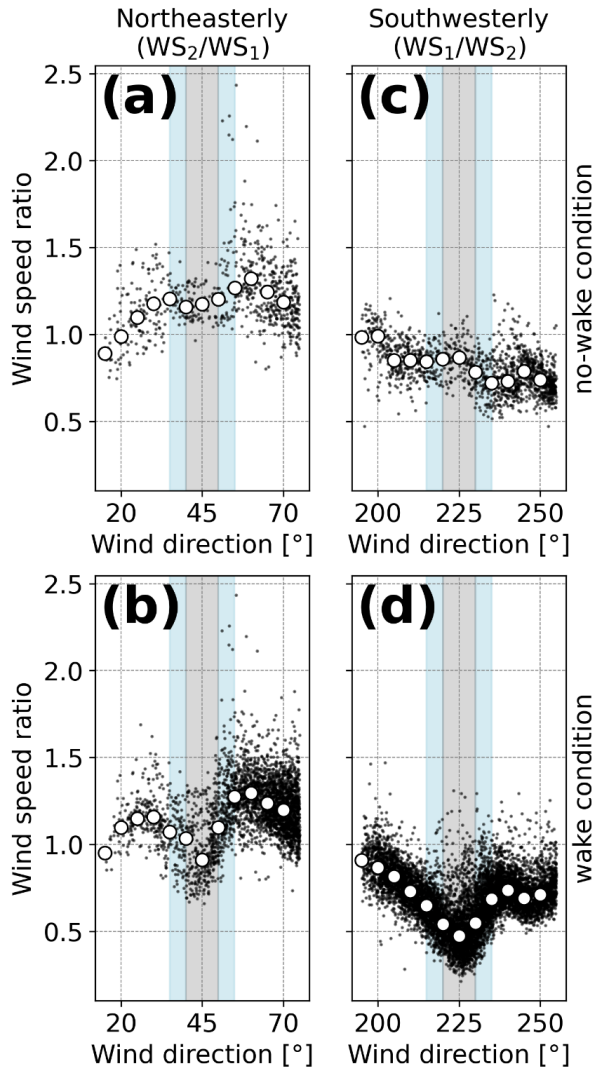
Figure 6. Wind speed ratios as a function of wind direction. Black dots denote 10-minute mean data and white circles denote
185 median values in every 5° bin. In (a) and (b), wind directions at WT2 are used. Note that the definition of the wind speed ratio
differs between (a) and (b). In (a), wind speed ratio is defined as the ratio of wind speed at wind turbine 2 (WS2) to that at wind
turbine 1 (WS1). In (b), wind speed ratio is defined as the ratio of WS1 to WS2. These definitions of the wind speed ratio are
common in the analyses to follow. Light blue shading indicates the range of wind direction with wake effects for (a) $45^\circ \pm 10^\circ$ and
(b) $225^\circ \pm 10^\circ$.

190

To clearly elucidate wake effects from the results of Fig. 6, we divide the data by the operating state of the upstream wind turbine.
We compare the wind speed ratio between no-wake conditions and wake conditions with a focus on the V-shaped curve at around
 $45^\circ \pm 10^\circ$ and $225^\circ \pm 10^\circ$ (Fig. 7). For northeasterly wind, the plots show no V-shaped curve and remain generally constant in no-
wake conditions (Fig. 7a). The wind speed ratios are higher than 1.0 with a median value of 1.18 at 45° and this means that the wind
195 speeds at WT2 are higher than those at WT1. In wake conditions (Fig. 7b), we can see significant reduction in wind speed ratio due
to the wake of WT1 with a maximum reduction of 23% at wind direction of 45°. For southwesterly wind, as is the case with Fig.
7a, the plots show no V-shaped curve and have almost the constant wind speed ratio in no-wake conditions (Fig. 7c). The median
value of wind speed ratio is 0.87 at 225°. The wind decelerates from the location of WT2 to the location of WT1 even without wakes
generated by WT2 because WT1 is positioned behind the hill. In wake conditions, wind speed ratio decreases to 0.47 from 0.87 in
200 no-wake condition and this means with a 46% reduction at 225° (Fig. 7d). This reduction observed for southwesterly wind is greater
than that observed for northeasterly winds. This reduction is larger than 22% from the previous work by Sasanuma and Honda



(2022) because they used the mean values and not the median values. From the above results, we find that the operation of the upstream wind turbine causes wind speed reduction at the downstream wind turbine and that the wake effect on the downhill side for southwesterly wind is more pronounced than that on the uphill side for northeasterly wind.



205

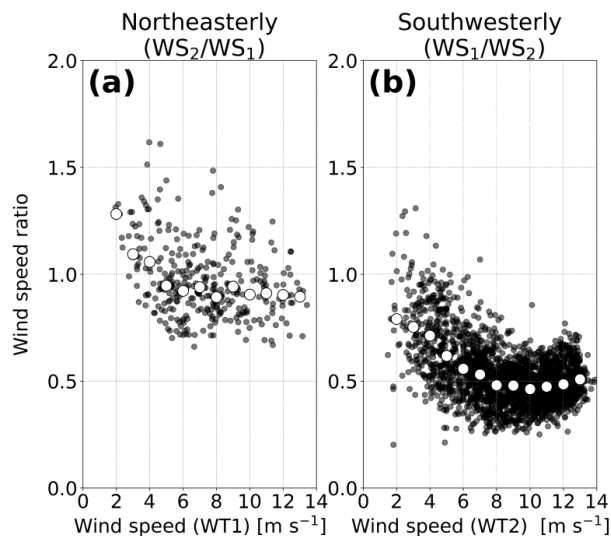
Figure 7. The same as in Fig. 6 but for being classified by the operating state of the upstream wind turbine in (a) (c) no-wake conditions and (b) (d) wake conditions for (a) (b) northeasterly wind and (c) (d) southwesterly wind. Light blue and gray shadings indicate the range of wind direction with wake effects. Gray shadings in the ranges of (a) (c) $45^{\circ} \pm 5^{\circ}$ and (b) (d) $225^{\circ} \pm 5^{\circ}$ represent the targeted ranges of wind direction for the analyses in Figs. 8, 9 and 10.

We examine the dependence of the magnitude of reduction in wind speed on inflow wind speed in wake conditions (Fig. 8). To exam the maximum wake effects, we focus on the ranges of wind direction for $45^{\circ} \pm 5^{\circ}$ and $225^{\circ} \pm 5^{\circ}$ (gray shading in Fig. 7). The horizontal axis shows wind speed at the upstream wind turbine when it is in operation. Figure 8 clearly shows the relationship between wind speed ratio and inflow wind speed for both northeasterly and southwesterly winds. The decrease in wind speed ratio means the increase in wake effect or the larger reduction in wind speed at the downstream wind turbine. For northeasterly wind, the

215

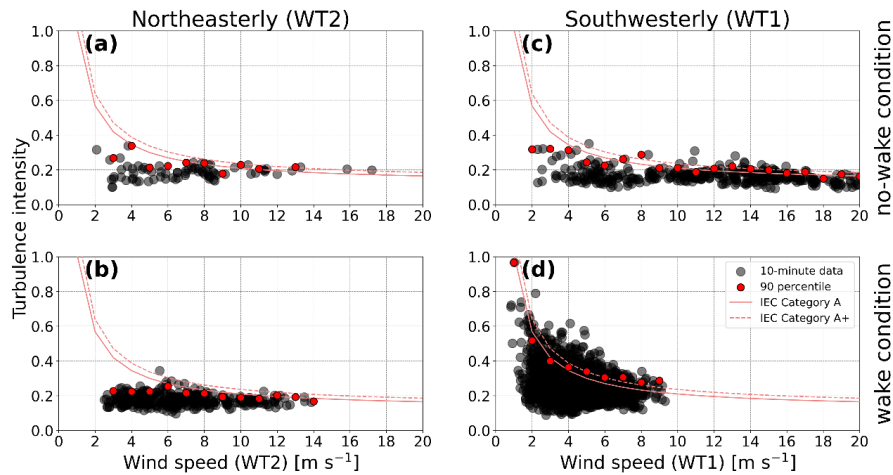


wind speed ratio decreases with inflow wind speed below a wind speed of 6 m s^{-1} , whereas, above 6 m s^{-1} , the wind speed ratio remains almost constant (Fig. 8a). For southwesterly wind, the wind speed ratio decreases with inflow wind speed and reach a minimum at 10 m s^{-1} (Fig. 8b). The gradual increase above 10 m s^{-1} suggests a start of control of the blade pitch angle. Thus, the wind turbine extracts the kinetic energy from the wind below the rated wind speed and the resulting momentum loss in the downstream induce the maximum wake effects. These results are consistent with those of Rhodes and Lundquist (2013) showing that the maximum reduction in wind speed occurs below the rated wind speed.



225 **Figure 8.** Wind speed ratio as a function of wind speed at the upstream wind turbine for (a) northeasterly wind and (b) southwesterly wind. Black dots denote 10-minute mean data and white circles denote median values in every 1 m s^{-1} bin.

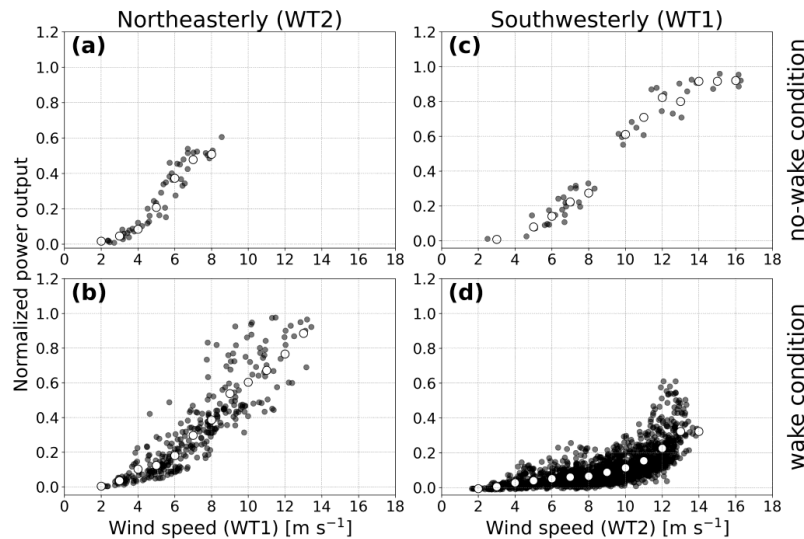
We investigate the wake effects on the turbulence intensity at the downstream wind turbine by comparing with the categories defined by the International Electrotechnical Commission (IEC, 2019). For northeasterly wind, the 90th percentile values of turbulence intensity hardly exceed the line of A+ category commonly in no-wake conditions and wake conditions (Figs. 9a and 9b). The wakes generated by WT1 contribute little to the increase in turbulence intensity at WT2. For southwesterly wind, the 90th percentile values of turbulence intensity for wind speeds greater than 7 m s^{-1} follows the line of A+ category in no-wake conditions (Fig. 9c). In wake conditions, wind speed at WT1 decreases to less than 10 m s^{-1} due to the wake generated by WT2 and the 90th percentile values of turbulence intensity follow the lines of A+ category and A category (Fig. 9d). However, the 10-minute mean data of turbulence intensity above the 90th percentile significantly exceeds the line of A+ category. The 10-minute mean data of turbulence intensity exceed 0.4 for wind speed less than 6 m s^{-1} . This is a noticeable difference between no-wake conditions and wake conditions. The wakes generated by WT2 cause high turbulence intensity at WT1 when the southwesterly wind blows (Sasanuma and Honda, 2022). These results suggest that the wake effects significantly vary depending on the topography.



240

Figure 9. Turbulence intensity as a function of wind speed in (a) (c) no-wake conditions and (b) (d) wake conditions for (a) (b) northeasterly wind and (c) (d) southwesterly wind. The data are extracted from the targeted range of wind direction, denoted by the gray shading in Fig. 7. The horizontal axis represents wind speed at (a) (b) WT2 and (c) (d) WT1. Black dots denote 10-minute mean data, and red circles denote 90th percentile values in every 1 m s^{-1} bin. The red dashed lines indicate standard curves of International Electrotechnical Commission (IEC) category A+ for very high turbulence, and the red solid lines indicate standard curves of IEC category A for high turbulence.

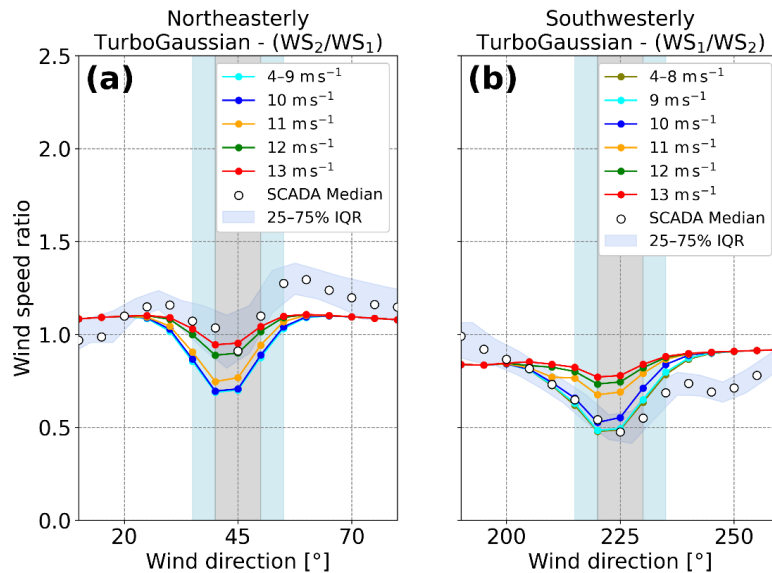
The impact of the wake on the power output of the downstream wind turbine is examined within the ranges of wind direction of $45^\circ \pm 5^\circ$ and $225^\circ \pm 5^\circ$ (Fig. 10). Note that the horizontal axis in Fig. 10 represents wind speed at the upstream wind turbine. For northeasterly wind, the power output at the downstream wind turbine WT2 is lower than expected from the wind speed at the upstream wind turbine WT1 (Figs. 10a and 10b). For example, in no-wake conditions, the normalized power output is approximately 0.5 at a wind speed of 8 m s^{-1} (Fig. 10a). In wake conditions, a wind speed of 9 m s^{-1} or a 12.5% increase in wind speed is required to generate the same power output (Fig. 10b). For southwesterly winds, the power output at the downstream wind turbine WT1 significantly decreases more than expected from the wind speed at the upstream wind turbine WT2 (Figs. 10c and 10d). For instance, the normalized power output is approximately 0.2 at 7 m s^{-1} in no-wake conditions (Fig. 10c). In wake conditions, a wind speed of 12 m s^{-1} or a 71% increase in wind speed is required to generate the same power output (Fig. 10d). At 14 m s^{-1} , the normalized power output in no-wake conditions is approximately 0.9 (Fig. 10c), whereas it decreases to approximately 0.3 in wake conditions (Fig. 10d). This result represents a 67% reduction in power output in case that we assume the same inflow wind speed at the downstream wind turbine. These findings suggest that wake effects have a more pronounced impact on power output for southwesterly winds than northeasterly winds. Even when the same wind speed is observed at the upstream wind turbine, the degree of reduction in wind speed or the resulting power output at the downstream wind turbine is different depending on the installation conditions of wind turbines.



265 **Figure 10.** Power output as a function of wind speed at the upstream wind turbine in (a) (c) no-wake conditions and (b) (d) wake
conditions for (a) (b) northeasterly wind and (c) (d) southwesterly wind. The horizontal axis represents wind speed at (a) (b) WT1
and (c) (d) WT2. Black dots denote 10-minute mean data, and white circles denote median values in every 1 m s^{-1} bin. The data are
extracted from the targeted range of wind direction, denoted by the gray shading in Fig. 7.

3.2 Simulated wake and wind flow

270 We validate the performance of 12 wake models implemented in PyWake by comparing the wind speed ratios computed from the
wake models with those from the SCADA data. We show the comparison results of wind speed ratio for different inflow wind
speeds by a typical wake model, Turbo Gaussian wake model for northeasterly and southwesterly winds (Fig. 11). The results of
wind speed ratio outside of wind direction with wake effects are computed by WASP CFD. The wind speed ratio decreases
275 significantly with decrease in inflow wind speed in the ranges of wind direction with wake effects for both northeasterly winds and
southwesterly winds. This means that significant reduction in wind speed occurs when inflow wind speed is small. The magnitude
of reduction in wind speed ratio are the same for wind speeds below 9 m s^{-1} for northeasterly wind (Fig. 11a) and below 8 m s^{-1} for
southwesterly wind (Fig. 11b), resulting the thrust curve used for the model (Fig. 5). The wake model shows the results close to
those from the SCADA data at inflow wind speed of $12\text{--}13 \text{ m s}^{-1}$ for northeasterly wind and at less than 9 m s^{-1} for southwesterly
280 wind, commonly true for the results from the other wake models (Figs. C1 and C2). All the wake models except the GCL wake
model tend to overestimate the reduction in wind speed for northeasterly wind. Most of the results underestimate the reduction in
wind speed in the southwesterly winds except Bastankhah and Turbo Gaussian wake models. We can conclude that the topographic
effects cause an opposite change in wake reproduction of wake models.

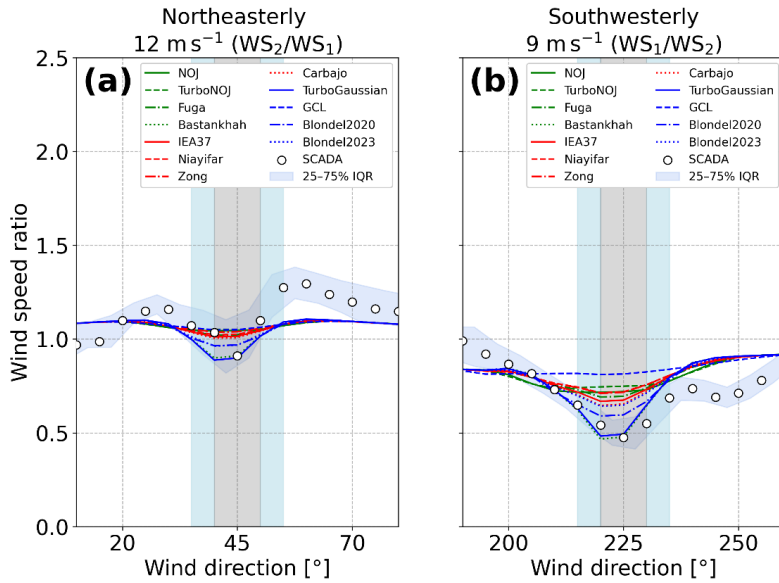


285

Figure 11. Wind speed ratio as a function of wind direction for (a) northeasterly wind and (b) southwesterly wind. The blue band denotes the range between lower and upper quartiles of the SCADA data and white circles denote median values in every 5° bin. Colored lines are results derived from an engineering wake model, TurboGaussian for every 1 m s⁻¹ for 4–13 m s⁻¹. The results for (a) 4–9 m s⁻¹ and (b) 4–8 m s⁻¹ are shown by one line because the differences are negligible. Light blue and gray shadings indicate the ranges of wind direction with wake effects.

We compare the wind speed ratio derived from the 12 wake models at the inflow wind speeds at 12 m s⁻¹ for northeasterly wind and 9 m s⁻¹ for southwesterly wind (Fig. 12). For northeasterly wind, most of the wake models underestimate the reduction in wind speed and represent weak wakes (Fig. 12a). For southwesterly wind, all the wake models except GCL wake model represent a reduction of wind speed ratio (Fig. 12b). Only Bastankhah and Turbo Gaussian wake models closely represent the minimum value of wind speed ratio derived from the SCADA data at 45° and 225°. To summarize the validation results from each wake model, we show the wind speed ratio for 12 wake models at 45° and 225° in Fig. 13. The order of the wake models according to the difference of the results between each wake model and the SCADA data are almost the same for northeasterly and southwesterly winds (Figs. 13a and 13b). The results from Turbo Gaussian and Bastankhah wake models agree with those from the SCADA data and Blondel2020 and Blondel2023 wake models follow the two wake models commonly for northeasterly and southwesterly wind. The differences from the SCADA data ranges from 2.3% to 21% for northeasterly wind and from 0.5% to 66% for southwesterly wind. The differences between the wake models are more prominent for southwesterly wind than for northeasterly wind. We need to pay attention to the accuracy of the reproduction and the choice of the wake models, as well as topographic situations.

300



305

Figure 12. Wind speed ratio as a function of wind direction for (a) northeasterly wind and (b) southwesterly wind. The blue band denotes the range between lower and upper quartiles of the SCADA data and white circles denote median values in every 5° bin. Colored lines are results derived from 12 wake models at (a) 12 m s⁻¹ and (b) 9 m s⁻¹. Light blue and gray shadings indicate the ranges of wind direction with wake effects.

310

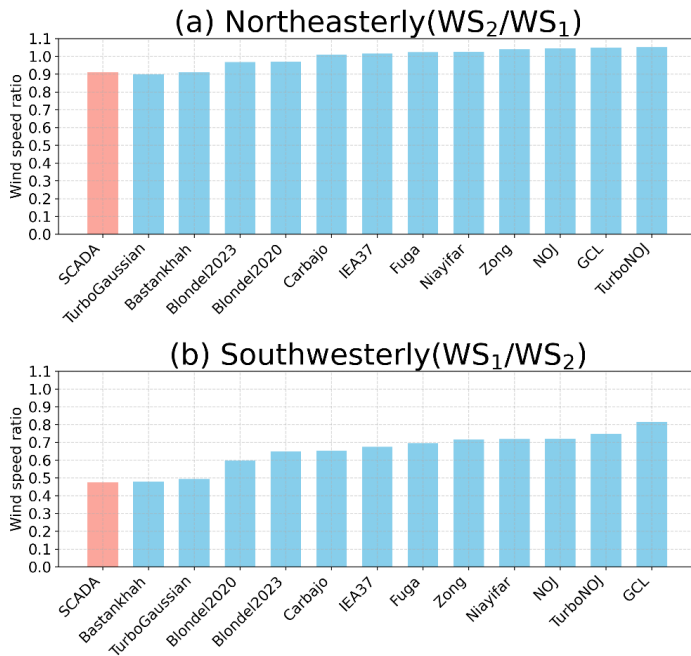


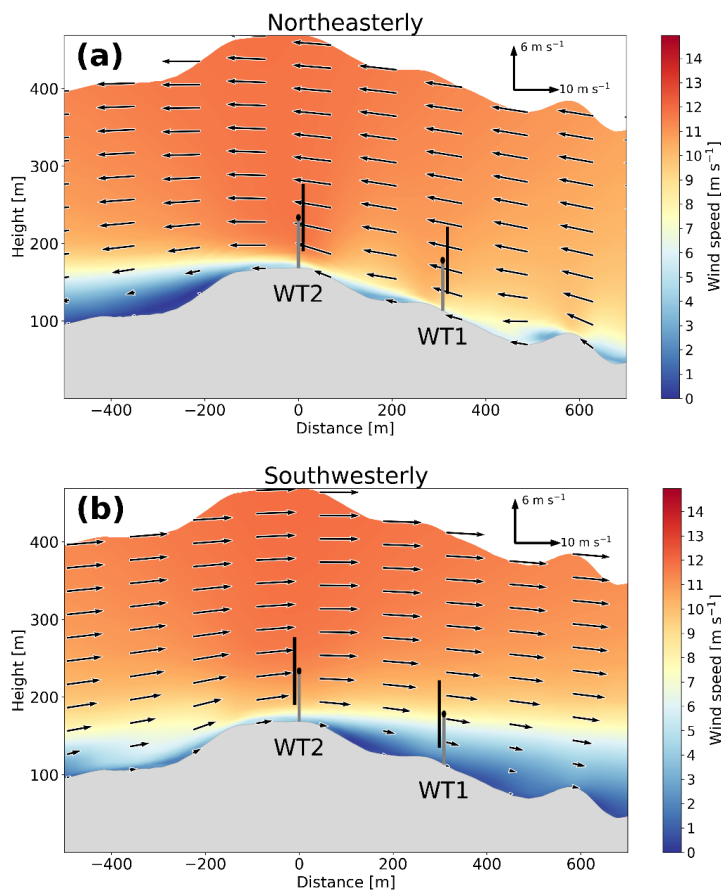
Figure 13. Wind speed ratio derived from the SCADA data and the engineering wake models for (a) northeasterly wind at 45° and (b) southwesterly wind at 225°.

315



To investigate the different wake effects between northeasterly and southwesterly winds, we study vertical cross sections of wind along the black dashed line in Fig. 1b computed by WAsP CFD without any wind turbines (Fig. 14). We can consider the path of wake generated by upstream wind turbine because the streamline is assumed to pass through the center of the turbine wake (Sesarego et al., 2020). For northeasterly wind, the wind reaches the hub height of WT2 from WT1 due to the wind ascending the hill (Fig. 14a). However, the wakes generated by WT1 might partly go through under the rotor surface and do not fully reach the rotor surface. Moreover, the flow accelerates on the top of the hill or around the location of WT2 and the accelerated wind blows through the rotor surface of WT2. Thus, the wind speed ratios are generally higher than 1.0 in no-wake conditions and the wake effects and reduction in wind speed at WT2 are limited even in wake conditions. For southwesterly wind, weak winds in the lee of the hill cover WT1 below the hub height and hit the underside of the rotor surface of WT1. In contrast, the strong winds on the top of the hill reach the hub height of WT1. The resulting strong vertical wind shear at the height of the rotor of WT1 contributes to the increase in turbulence. Moreover, no acceleration occurs in the lee of the hill or WT2. Thus, the wind speed ratios are generally lower than 1.0, and the wake effects are more enhanced for southwesterly wind than for northeasterly wind. Further studies are necessary to examine whether the wake generated by WT2 completely reach the rotor of WT1, possibly due to the weak descending wind.

330



335

Figure 14. Vertical cross sections of horizontal wind speed (color shading) and wind vectors on the cross section along the black dashed line in Fig. 1b for (a) northeasterly wind and (b) southwesterly wind. The data outputs from WAsP CFD are available up to 300 m and the white part is outside of the data outputs. Note that although we show the locations of wind turbines, these results include no wake effects of the wind turbines.



4 Summary and conclusions

We have investigated the bidirectional wake effects between the two wind turbines in complex terrain at a site in northern Japan using the SCADA data and validated the performance of the wake models. We have addressed the two issues: (1) to identify the wake effects for northeasterly and southwesterly winds in term of reduction in wind speed, turbulence intensity, and power output. (2) to validate the performance of the wake models and impacts of the topography on the simulated wakes. The main results are summarized as follows.

(1) Using the SCADA data, we detected wake effects from the differences in the wind speed ratio between no-wake conditions and wake conditions. These conditions are classified by the operating state of the upstream wind turbine on the basis of the blade pitch angle. The upstream wind turbine reduces wind speed at the downstream wind turbine for both northeasterly and southwesterly winds. For northeasterly wind, the wind speed ratio in no-wake conditions generally exceeds 1.0 and the maximum reduction in wind speed due to the wake is 23%. For southwesterly wind, the wind speed ratio in no-wake conditions is generally below 1.0 and the maximum reduction in wind speed due to wake is 46%. Wake effects for southwesterly wind are enhanced more than for easterly wind because of the weak winds in the lee of the hill. Turbulence intensity at the downstream wind turbine increases due to the wake for southwesterly wind. The upper 10% data of turbulence intensity exceed the level of A+ category induced by wake generated by the upstream wind turbine. The decrease in power output at the downstream wind turbine for southwesterly wind shows more pronounced impact than for northeasterly wind. From this investigation using SCADA data, the study revealed wake effects of the surrounding terrain and inflow wind speed. These results indicate the importance to consider the combined effects of wakes and topography.

(2) We compared the wind speed ratios derived from 12 wake models in PyWake and examined wind fields by WASP CFD. The wind speed ratios derived from the wake models show strong dependence on inflow wind speed. This dependence reflects the thrust curve used for wake computation in the wake models. The wake models commonly overestimate the reduction in wind speed for northeasterly wind and underestimate it for southwesterly wind. Additional effects of topography to the wake effects cause opposite changes in the simulated wakes. The wake models with high reproducibility are Turbo Gaussian and Bastankhah models. These models represent the minimum wind speed ratio or maximum reduction in wind speed close to the observations when inflow wind speeds are 12 m s^{-1} for easterly wind and 9 m s^{-1} for westerly wind. We can conclude that the topographic effects cause an opposite change in wake reproduction.

By analysing the SCADA data, this study reveals the fundamental characteristics of bidirectional wake effects over complex terrain. Using the SCADA data provides much information. The method used for detecting wake effects demonstrates the potential to utilize the SCADA data collected during downtime of wind turbines, such as maintenance periods and curtailment periods. Although this study focuses on onshore wind turbines, the findings provide important suggestions for offshore wind turbines near the coast influenced by terrain effects and for wind power plants subject to multiple wake interactions. We further need to investigate the uncertainty of wake effects in terms of the variance of data in wind speed ratio. To deepen our understanding of terrain effects on wakes, further work should incorporate atmospheric stability into analyses of the flow. In addition, increased turbulence intensity owing to wakes increases the risks of fatigue loads and shortens the lifespan of wind turbines. Assessing fatigue loads on downstream wind turbines through aeroelastic simulation would provide valuable insights.

Appendix A: Methodology to correct SCADA data

For the correction of measurement data on the nacelle, referring the observed values without the influence of rotor rotation is common. Pedersen et al. (2015) suggested a method that measures wind flow without turbulence due to turbine rotation using a spinner anemometer mounted on the nacelle top. Mittelmeier and Kühn (2018) investigated improving the yaw misalignment by utilizing wind flow measurements from external devices, such as two cup-type anemometers, a wind direction vane, and a mast. Another way is to estimate inflow wind based on deep learning using doppler LiDAR in upstream side and nacelle wind data



(Shimada and Otake, 2021). In this paper, we suggest the way to correct the wind data measured on the nacelle without any external devices by defining four operating conditions between two turbines. To evaluate wind direction error due to turbine rotation
 380 quantitatively, we formalize the inflow wind direction in

$$WD_{R,i} = WD_{M,i} + \Delta\theta_i \quad (A1)$$

where $WD_{R,i}$ is the inflow wind direction of turbine i not affected by the turbine's rotation, $WD_{M,i}$ is the turbine i 's wind direction measured on the nacelle, and correction factor $\Delta\theta_i$. When the turbine is not operating, $\Delta\theta_i = 0$ therefore $WD_{R,i} = WD_{M,i}$. Based on Eq. (A1), we see wind direction difference for all of the two turbines operating conditions. The weighted methods for frequency
 385 wind direction and operation status are considered. Using this method, 5.1°-6.4° are considered as wind direction errors due to turbine's rotation effect.

We formalize the incoming wind speed considering of wind speed error in

$$WS_{R,i} = \kappa_i * WS_{M,i,on} \quad (A2)$$

where $WS_{R,i}$ is the inflow wind speed of turbine i , which is not affected by the turbine's rotation, $WS_{M,i,on}$ is the operating turbine
 390 i 's wind speed measured on the nacelle, and κ_i is the turbine i 's wind speed error. When the turbine is not operating, $\kappa_i = 1$ and $WS_{R,i} = WS_{M,i,off}$. Based on Eq. (A2), the wind speed ratio between two turbines can be expressed in

$$WS_{R,1}/WS_{R,2} = WS_{M,1}/WS_{M,2} * \tilde{\kappa}_1/\tilde{\kappa}_2 \quad (A3)$$

Using this method, 0.98-1.00 are considered as wind speed ratio errors due to turbine's rotation effect. Compared with wind direction, effect of turbine rotation for wind speed is smaller.

395

Appendix B: 12 wake models names

We present 12 wake models used in this study in Table. 1.

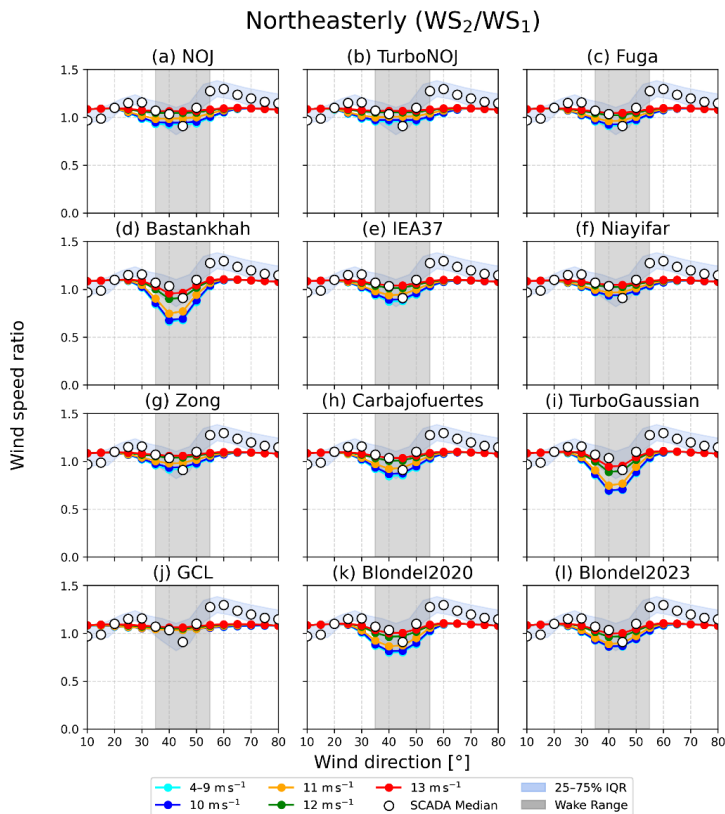
Table B1. Abbreviations and full names for 12 wake models

Abbreviation	Full name
NOJ	NOJDeficit
TurboNOJ	TurboNOJDeficit
Fuga	FugaDeficit
Bastankhah	BastankhahGaussianDeficit
IEA37	IEA37SimpleBastankhahGaussianDeficit
Niayifar	NiayifarGaussianDeficit
Zong	ZongGaussianDeficit
Carbajofuertes	CarbajofuertesGaussianDeficit
TurboGaussian	TurboGaussianDeficit
GCL	GCLDeficit
Blondel2020	BlondelSuperGaussianDeficit2020
Blondel2023	BlondelSuperGaussianDeficit2023

400

Appendix C: Wind speed reduction using 12 wake models

We show the results of wind speed reduction using 12 wake models for northeasterly winds and southwesterly winds in Figs. C1 and C2. In northeasterly winds, some of the models underestimate the wind speed reduction (Figs. C1a, C1b, C1f, and C1j). For southwesterly winds, most of the models underestimate the wind speed reduction excluding Figs. C2d and C2i.



405

Figure C1. Wind speed ratio for 12 wake models for northeasterly wind. The blue band denotes the range between lower and upper quartiles of the SCADA data and white circles denote median values in every 5° bin. Colored lines are results derived from each wake model for every 1 m s⁻¹ for 4–13 m s⁻¹.

410

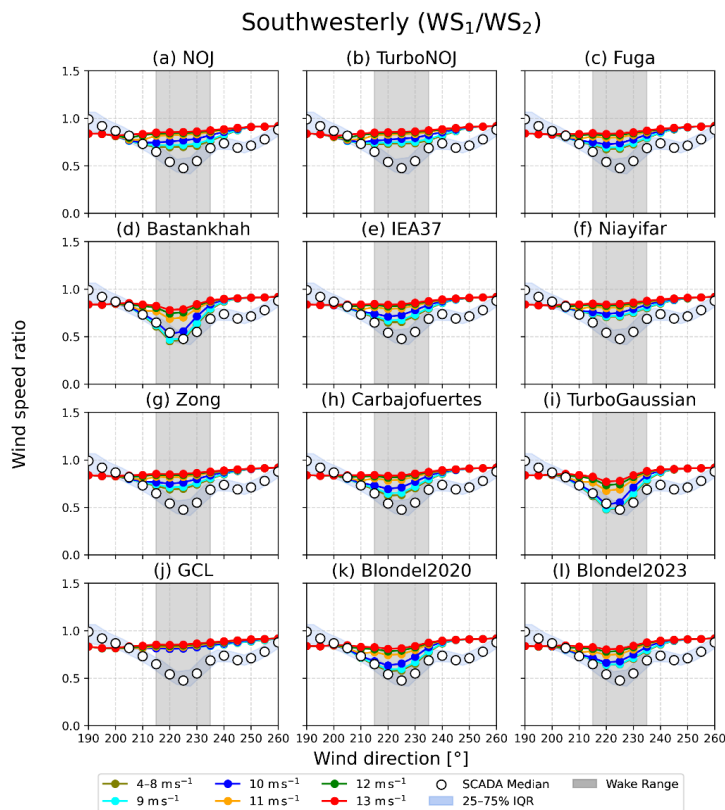


Figure C2. The same as in Fig. C1 but for southwesterly wind.

Code availability

415 We used an open source in PyWake 2.5 (<https://topfarm.pages.windenergy.dtu.dk/PyWake/> (last access: 17 July 2025)) and WAsP
 12 (<https://www.wasp.dk/software/wasp-cfd> (last access: 17 July 2025)) in this study.

Data availability

The SCADA data were provided by Tsugaru Peninsula Eco Energy Co., Ltd. and were unavailable to the public.

420

Author contribution

Writing (original draft preparation) and visualization: NS, and TS. Writing (review and editing): AH, CB, NT, MG, and MN. Methodology and investigation: NS, AH, MG, and TS. Software: NS and MN. Conceptualization: NS, AH, and TS. All authors contributed with critical feedback on this research and have read and agreed to the published version of the paper.



425 **Competing interests**

The authors declare that they have no competing interests.

Acknowledgments

We would like to express my gratitude to the staff of Tsugaru Peninsula Eco Energy Co., Ltd. and the staff of Japan Steel Works, Ltd. for providing the observational data. We appreciate Mr. Mads Mølgaard Pedersen in analysing WAsP CFD, PyWake and Ms. Ginka Georgieva Yankova for data uncertainty analysis. This research was supported by the JST Challenging Research Program for Next-Generation Researchers JPMSP2152.

References

- Astolfi, D., Castellani, F., and Terzi, L.: A study of wind turbine wakes in complex terrain through RANS simulation and SCADA data, *J. Sol. Energy Eng.*, 140, 031001, <https://doi.org/10.1115/1.4039093>, 2018.
- Bastankhah, M., and Porté-Agel, F.: A new analytical model for wind-turbine wakes. *Renewable Energy*, 70, 116-123. <https://doi.org/10.1016/j.renene.2014.01.002>, 2014.
- Bechman, A.: WAsP CFD A new beginning in wind resource assessment, Tech. rep., Risø National Laboratory, Denmark, 2012.
- Carbajo Fuertes, F., and Markfort, C. D.: Wind Turbine Wake Characterization with Nacelle-Mounted Wind Lidars for Analytical Wake Model Validation. *Remote Sensing*, 10, 668. <https://doi.org/10.3390/rs10050668>, 2018.
- Dilip, D. and Porté-Agel, F.: Wind turbine wake mitigation through blade pitch offset, *Energies*, 10(6), 757, <https://doi.org/10.3390/en10060757>, 2017.
- Duncan Jr., J. B., Hirth, B. D., and Schroeder, J. L.: Exploring the complexities associated with full-scale wind plant wake mitigation control experiments, *Wind Energ. Sci.*, 5, 469–488, <https://doi.org/10.5194/wes-5-469-2020>, 2020.
- El-Asha, S., Zhan, L., and Iungo, G. V.: Quantification of power losses due to wind turbine wake interaction through SCADA, meteorological and wind LiDAR data, *Wind Energy*, 20, 1823–1839, <https://doi.org/10.1002/we.2123>, 2017.
- Enomoto, S., Inomata, N., Yamada, T., Chiba, H., Tanikawa, R., Oota, T., and Fukuda, H.: Prediction of power output from wind farm using local meteorological analysis, in: *Proceedings of the European Wind Energy Conference*, Copenhagen, Denmark, 2-5 June 2001, 749-752, ISBN 3-936338-09-4, 2001.
- Fujikawa, T., Iwasaki, N., Suguro, Y., Iwanaga, Y., and Shibata, M.: Mitsubishi high efficiency large capacity wind turbines, Mitsubishi heavy industries, Ltd. Technical review, 39, 101-106, <https://www.researchgate.net/publication/237268778>, 2002.
- Geospatial Information Authority of Japan: <https://maps.gsi.go.jp/>, last access: 9 April 2025.
- Göçmen, T., Laan, P. V. D., Réthoré, P., Diaz, A. P., Larsen, G. C., and Ott, S.: Wind turbine wake models developed at the technical university of Denmark: A review. *Renewable and Sustainable Energy Reviews*, 60, 752-769. <https://doi.org/10.1016/j.rser.2016.01.113>, 2016.
- Han, X., Liu, D., Xu, C., and Shen, W., Z.: Atmospheric stability and topography effects on wind turbine performance and wake properties in complex terrain, *Renewable Energy*, 126, 640-651, <https://doi.org/10.1016/j.renene.2018.03.048>, 2018.
- Hansen, K.S., Larsen, G.C., Menke, R., Vasiljevic, N., Angelou, N., Feng, J., Zhu, W.J., Vignaroli, A., Liu, W., Xu, C., and Shen, W.Z.: Wind turbine wake measurement in complex terrain. *J. Phys. Conf. Ser.* 753, 1-10, <https://doi.org/10.1088/1742-6596/753/3/032013>, 2016.
- Hasegawa, Y., Kikuyama, K., Imamura, H., Inomata, N., Suzuki, H., and Ishikawa, H.: Fundamental study for estimation of wind energy resources (Wind Measurements at Tappi Wind Park), *Nihon kikai gakkai ronbunshu, B Hen/Transactions of the Japan Society of Mechanical Engineers, Part B*, 69, 2052-2058, 10.1299/kikaib.69.2052, 2003.



- IEC – International Electrotechnical Commission: IEC 61400-1: Wind energy generation systems – Part 1: Design requirements, 465 4th Edn., Geneva, Switzerland, 2019.
- Inomata, N., Tsuchiya, K., and Yamada, S.: Measurement of stress on blade of NEDO's 500 kW prototype wind turbine, *Renewable Energy*, 16, 912-915, [https://doi.org/10.1016/S0960-1481\(98\)00309-7](https://doi.org/10.1016/S0960-1481(98)00309-7), 1999.
- Mittelmeier, N., Allin, J., Blodau, T., Trabucchi, D., Steinfeld, G., Rott, A., and Kühn, M.: An analysis of offshore wind farm SCADA measurements to identify key parameters influencing the magnitude of wake effects, *Wind Energ. Sci.*, 2, 477–490, 470 <https://doi.org/10.5194/wes-2-477-2017>, 2017.
- Mittelmeier, N., and Kühn, M., Determination of optimal wind turbine alignment into the wind and detection of alignment changes with SCADA data. *Wind Energ. Sci.*, 3, 395–408. <https://doi.org/10.5194/wes-3-395-2018>, 2018.
- Pedersen, M. M., van der Laan, P., Friis-Møller, M., Forsting, A. M., Riva, R., Romàn, L. A. A., Risco, J., C., Quick, J., Christiansen, J. P. S., Olsen B. T., Rodrigues, R. V., and Réthoré, P. E., DTU WindEnergy/PyWake: PyWake (v2.5.0), 475 <https://doi.org/10.5281/zenodo.6806136>, 2023.
- Rhodes, M. E., and Lundquist, J. K.: The effect of wind-turbine wakes on summertime US midwest atmospheric wind profiles as observed with ground-based Doppler lidar, 149, 85-103, <https://doi.org/10.1007/s10546-013-9834-x>, 2013.
- Sasanuma, N., and Honda, A.: Study on wind characteristic and wind wake effect in complex terrain, *Journal of wind engineering*, 27, 294-302, https://doi.org/10.14887/windengresearch.27.0_294, 2022.
- 480 Sasanuma, N., and Honda, A.: Observation survey on wind turbines installed close to complex terrain: the effects terrain and wind turbine wake, *Journal of wind engineering*, 28, 267-275, https://doi.org/10.14887/windengresearch.28.0_267, 2024.
- Sassarego, M., Feng, J., Friis-Møller, M., Xu, Y., Xu, M. and Shen, W., Z.: Development of a streamline wake model for wind farm performance predictions, *J. Phys. Conf. Ser.*, 1618, 062027, 10.1088/1742-6596/1618/6/062027, 2020.
- Sayre, R., Frye, C., Karagulle, D., Krauer, J., Breyer, S., Aniello, P., Wright, D., J., Payne, D., Adler, C., Warner, H., VanSisine, 485 D., P., and Cress, J.: A new high-resolution map of world mountains and an online tool for visualizing and comparing characterizations of global mountain distributions, *Mountain research and development*, 38, 240-249, <https://doi.org/10.1659/MRD-JOURNAL-D-17-00107.1>, 2018.
- Shimada, S., and Otake, Y.: Inflow Wind estimation based on deep learning for yaw misalignment, *J. Japan Wind Energy Assoc.*, 46, 1-6, https://doi.org/10.11333/jwearonbun.46.2_11, 2022.
- 490 Shimada, T., Sawada, M. and Iwasaki, T.: Indices of cool summer climate in northern Japan: Yamase indices, *J. Meteor. Soc. Japan*, 92, 17-35, 10.2151/jmsj.2014-102, 2014.
- Troldborg, N., Andersen, S. J., Hodgson, E. L., and Meyer Forsting, A.: Brief communication: How does complex terrain change the power curve of a wind turbine?, *Wind Energ. Sci.*, 7, 1527–1532, <https://doi.org/10.5194/wes-7-1527-2022>, 2022.
- Uchida, T., Takakuwa, S., Watanabe, K., Hasegawa, S., Baba, Y., Murakami, R., Yamasaki, M., and Hideka, K.: Numerical 495 visualization of wind turbine wakes using passive scalar advection-diffusion equation and its application for wake management, *Wind Engineering*, 46, 1870-1887, 10.1177/0309524X221113011, 2022.
- Ushiyama, I.: Wind energy activities in Japan, *Renewable Energy*, 16, 811-816, [https://doi.org/10.1016/S0960-1481\(98\)00261-4](https://doi.org/10.1016/S0960-1481(98)00261-4), 1999.
- Yamaguchi, A., Ishihara, T., and Fujino, Y.: Applicability of linear and nonlinear wind prediction models to wind flow in complex 500 terrain, in: *Proceedings of The World Wind Energy Conference and Exhibition*, Berlin, Germany, 3-8 July 2002, 1-4, <https://www.researchgate.net/publication/266863617>, 2002.
- Yamaguchi, A., Tavana, A., and Ishihara, T.: Assessment of wind over complex terrain considering the effects of topography, Atmospheric stability and turbine wakes, *Atmosphere*, 15, 723, <https://www.mdpi.com/2073-4433/15/6/723>, 2024.